

Synthesis and Characterization of $K_2Ln_{2/3}Ta_2O_7 \cdot nH_2O$ (Ln= La, Pr, Nd), Layered Tantalates Photocatalysts for Water Splitting.

Hoover Valencia-Sanchez,^{1,5*} Heriberto Pfeiffer,² Dwight Acosta,³ Alicia Negron-Mendoza⁴ and Gustavo Tavizon¹

¹ Facultad de Química.

² Instituto de Investigaciones en Materiales.

³ Instituto de Física.

⁴ Instituto de Ciencias Nucleares; Universidad Nacional Autónoma de México. Ciudad Universitaria, C.P. 04510, México D.F.

⁵ Permanent address: Escuela de Química, Universidad Tecnológica de Pereira, Carrera 27 10-02 Los Alamos, C. P. 660003, Pereira-Colombia, Tel. (+57)63137242, hvalencia@utp.edu.co

Received July 7th, 2014; Accepted January 27th, 2015

Abstract. Three compounds of the $K_2Ln_{2/3}Ta_2O_7$ (Ln = La, Nd, Pr) cation-deficient Ruddlesden-Popper series were prepared by the Pechini (polymeric complex) method. The crystal structures of the hydrated form of these compounds were determined by Rietveld analysis of the X-ray powder diffraction data and High Resolution Transmission Electron Microscopy (HRTEM). The samples were also analyzed to determine specific area (BET), degree of hydration (TGA), and photocatalytic activity for hydrogen evolution from water and aqueous methanol solution.

Key words: Photocatalyst, Water Splitting, Tantalates, Ruddlesden-Popper, Hydrogen production.

Resumen. Tres compuestos del tipo $K_2Ln_{2/3}Ta_2O_7$ (Ln = La, Nd, Pr) de la serie de Ruddlesden-Popper deficientes de cationes fueron preparados por el método de Pechini (complejo polimerizable). Las estructuras cristalinas de los compuestos hidratados fueron determinadas por análisis de Rietveld de los patrones de difracción de rayos X y mediante microscopía electrónica de alta resolución (HRTEM). Las muestras también fueron analizadas para determinar su área superficial (BET); grado de hidratación (TGA), y actividad fotocatalítica en la producción de hidrógeno a partir de agua y de soluciones metanol/agua.

Palabras Clave: Fotocatalizadores, Disociación del agua, Tantalatos, Ruddlesden-Popper, Producción de Hidrógeno.

Introduction

Tantalum-oxide based compounds crystallizing in the Ruddlesden-Popper (RP) structure[1] have recently attracted much attention due to their ion-exchange[2]–[5] (96 and intercalation[6]–[8] properties and as photocatalysts for hydrogen generation from water splitting[9]–[11]. Additionally, high proton conductivity has been recently reported[12] in randomly oriented grains of $H_2SrTa_2O_7$ and $SrTa_2O_6$. In their anhydrous form, the $K_2[Ln_{3/2}Ta_2O_7]$ RP tantalates correspond to the formula $A'_2[A_{n-1}B_nO_{3n+1}]$, where A' is often an alkali metal, A is a rare earth metal, B is a transition metal, and n defines the number of BO_6 octahedra forming perovskite layers[13]. In this structure there are two A' interlayer cations per formula unit interconnecting the n perovskite sheets. Most of the compounds of the RP series with B=Ti and/or Ta crystallize in the space group (SG) I4/mmm (No. 139), which consists of perovskite blocks separated by rock-salt type $A'O$ blocks. This structure produces a staggered arrangement in which two contiguous perovskite blocks are shifted by $(a+b)/2$ in the crystal cell. During intercalation of water into the RP structure, the water molecules form new layers inside the rock-salt type block[14], and a structural change from the I4/mmm to the P4/mmm (No. 123) SG occurs[15]. As reported for several layered tantalates with photocatalytic water

splitting activity[9],[10],[16],[17], the interlayer hydration plays a key role because the intercalated water molecules are accessible to the active sites responsible for the photocatalytic reaction. The number of publications on the photocatalytic activity of layered tantalates has increased in recent years, such as Kudo et al.[18] reported. These new semiconductors are laminar compounds exhibiting a layered structure in which perovskite blocks consisting of TaO_6 octahedra are thought to be responsible of such photoactivity. One of them, the $NaTaO_3$ has the highest quantum yield in the photocatalytic reaction that splits water into H_2 and O_2 . This compound was studied using different lanthanide doping such as: La, Pr, Nd, Sm, Gd, Tb and Dy[19]. $NaTaO_3$ presents a quantum yield of 56% at 270 nm when it is doped with lanthanum and Ni-loading ($NaTaO_3:La$ (2%) NiO (0,2 % w))[20],[21]. On the other hand, the undoped compound, $NaTaO_3:NiO$ (0,05 %w), presented a yield of 28% at 270 nm (surface specific area of 0,52 m^2/g) as reported Kato et al.[22]. The significant decrease in particle size and a topography in which terraces predominate separating active sites for oxidation and reduction are thought to be the main responsible factors of such phenomenon[23].

With the aim of investigating the synthetic route and the main crystal features of hydrated layered tantalates and to explore the effect of the partially filled 4f shell cations (Pr, Nd)

on photocatalytic activity for hydrogen evolution of the RP tantalates, a study of the $K_2Ln_{2/3}Ta_2O_7$ ($Ln = La, Pr, Nd$) series of compounds is presented. These compounds were synthesized via the Pechini method (PC) that results in good crystallinity of the samples and higher or equal specific areas than the synthesized by the solid-state reaction method. These characteristics are important in the heterogeneous photocatalytic process of these systems. The compounds synthesized in this work are lanthanide-deficient (1/3 per formula unit) and, as reported for the $RbLnTa_2O_7$ tantalate[24], the role played by these lanthanides in the neighborhood of the TaO_6 octahedra cannot be considered as that of “spectator” in the photocatalytic activity behavior of these layered perovskite tantalates.

Results and Discussion

XRD patterns of the hydrated phase (HP) of $K_2La_{2/3}Ta_2O_7$ (LaN2), $K_2Pr_{2/3}Ta_2O_7$ (PrN2), and $K_2Nd_{2/3}Ta_2O_7$ (NdN2) are shown in **Fig. 1**. In the **Table 1**, a list of reflections that correspond to diffraction pattern of the **Fig 1** is presented. The reflections marked with (*) in **Table 1**, contribute to the total intensity and the observed reflection corresponds to the sum of several reflections. For example, the first reflection should be assigned to the 003, 010 and 011 contributions. The second one results from the 013, 110, 111 and 014 reflections. The formation of the PR phases were also supported by HRTEM (see below). Likewise, the wide character of the main reflections observed in these patterns must be associated with the small size of crystallites obtained by the Pechini method of synthesis. In this synthetic route, an important element to consider refers to the calcination temperature because once this exceeds $900^\circ C$, undesired tungsten-bronze type compounds appear in the XRD patterns[25]. Several authors have referred to the appearance of tungsten bronzes, obtained by the solid-state reaction method[26]–[28].

To determine the number of hydrating water molecules in samples, dynamic thermogravimetric analysis (TGA) was performed and the compounds were heated under airflow from $25^\circ C$ to $1000^\circ C$ ($10^\circ C/min$). To consider only the water molecules intercalated into the crystal structure, without taken into account the water molecules on the crystal surface, the weight-loss was considered from $100^\circ C$. According to these thermogravimetric analyses, the number of hydration water molecules for LaN2, PrN2 and NdN2 is 2.5, 1.8 and 0.83, respectively. A plot of this thermal behavior is presented in **Fig. 2**. As observed in this plot, the number of intercalated water molecules in these layered structure compounds is different for each lanthanide, decreasing in the order $LaN2 > PrN2 > NdN2$.

As previously reported for alkaline laminar tantalates (except Li[10],[16],[17],[27], Cs and Rb[29]), these compounds exhibit spontaneous water intercalation when exposed to air under room temperature[27],[28],[30]. For the anhydrous

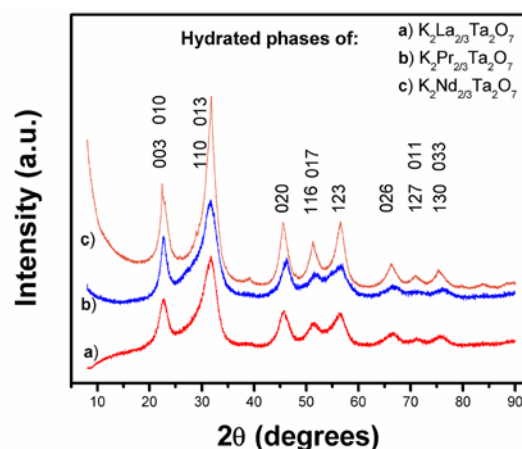


Fig. 1. XRD patterns of the HP of a) $K_2La_{2/3}Ta_2O_7$ (LaN2); b) $K_2Pr_{2/3}Ta_2O_7$ (PrN2) and d) $K_2Nd_{2/3}Ta_2O_7$ (NdN2), obtained at room temperature. The hkl Miller indices are indicated above the main reflections. The peak width is associated to the loss of crystallinity and very small size of crystallites. No additional reflections as those assigned to tungsten-bronze phases were detected.

phase of $K_2La_{2/3}Ta_2O_7$, Crosnier-Lopez et al[27] determined an $I4/mmm$ space group with $a = 3.9679\text{\AA}$ and $c = 22.0807\text{\AA}$ crystal cell parameters. Water intercalation of this compound is extremely rapid and one structural transition was observed from the body centered ($I4/mmm$) to a primitive lattice ($P4/mmm$) in the hydrate form of this compound, $K_2La_{2/3}Ta_2O_7 \cdot 2H_2O$. For this compound the cell parameters are $a = 3.9427\text{\AA}$ and $c = 12.887\text{\AA}$ [27]. As occurs in other laminar compounds of the Ruddlesden-Popper series as $K_2Nd_2Ti_3O_{10}$, water intercalation produces a change in the symmetry due to an $(a+b)/2$ sliding of the central slab relative to the adjacent slabs[31]. The SG for all the $LnN2$ ($Ln = La, Pr$ and Nd) hydrated phases is $P4/mmm$ and the diffraction patterns are presented in **Fig. 1**.

Crystal structure of $K_2La_{2/3}Ta_2O_7$ has been previously reported by Crosnier-Lopez et al[27] through Rietveld refinements of XRD data. In the present work, Rietveld refinement of the hydrated form of this phase is presented, and this study has been extended to include the Pr and Nd cations in the crystal unit cell (see **Fig. 3**). For the Rietveld analysis the $P4/mmm$ SG was attempted[4], and the water molecule position was the 2e Wyckoff site ($0, 1/2, 1/2; 1/2, 0, 1/2$); however, its occupancy was not refined and the different water stoichiometries of the compounds correspond to those estimated from thermal analysis. However, the values of the isotropic thermal parameters for O_w (oxygen atom of the water molecule) are acceptable for LaN2, PrN2 and NdN2, when considering the interlayer distance in which those molecules are located. Site-occupancy refinements of Ta and O were also omitted because of the low volatility (and very low solubility in water) of the metal-oxide, and stability of the oxidation state of Ta. Considering the ab plane as that formed by the O(2) at the 4i Wyckoff position, Ta rises from this plane and the Ta-O(2)-Ta angle is 163.7° (LaN2); 163.56° (PrN2) and

Table 1. Reflections for the diffraction pattern to $K_2La_{2/3}Ta_2O_7$, $K_2Pr_{2/3}Ta_2O_7$ and $K_2Nd_{2/3}Ta_2O_7$ compounds of **Fig 1**.

Miller Indices (hkl)	$K_2La_{2/3}Ta_2O_7$		$K_2Pr_{2/3}Ta_2O_7$		$K_2Nd_{2/3}Ta_2O_7$	
	2 θ (Degrees)	Distance (Å)	2 θ (Degrees)	Distance (Å)	2 θ (Degrees)	Distance (Å)
003	19.481	4.5529	19.419	4.5673	21.471	4.1353
010*	22.608	3.9298	22.520	3.9449	22.283	3.9864
011	23.538	3.7766	23.448	3.7909	23.421	3.7953
013*	30.014	2.9749	29.905	2.9855	31.138	2.8700
110*	32.187	2.7788	32.060	2.7895	31.718	2.8188
111	32.865	2.7230	32.736	2.7334	32.549	2.7488
014	34.777	2.5776	34.653	2.5865	36.683	2.4479
020*	46.162	1.9649	45.975	1.9725	45.469	1.9932
007	46.504	1.9512	46.349	1.9574	51.525	1.7723
021	46.665	1.9449	46.476	1.9523	46.086	1.9680
023	50.552	1.8041	50.351	1.8108	50.810	1.7955
116*	51.880	1.7610	51.689	1.7670	55.036	1.6672
017	52.305	1.7477	52.120	1.7534	56.805	1.6194
123*	56.046	1.6395	55.817	1.6457	56.136	1.6371
117	57.682	1.5969	57.469	1.6023	61.783	1.5004
026*	62.379	1.4874	62.133	1.4927	64.931	1.4350
127*	72.297	1.3059	72.002	1.3105	75.594	1.2569
011*	73.319	1.2902	73.044	1.2943	81.127	1.1845
033*	75.454	1.2589	75.119	1.2633	75.018	1.2651
130*	76.611	1.2427	76.264	1.2475	75.331	1.2606

*Reflections that contribute more intensity in the **Fig 1**.

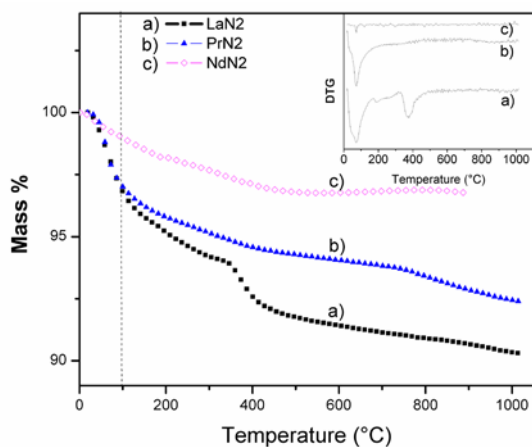


Fig. 2. Thermogravimetric analysis of the $K_2Ln_{2/3}Ta_2O_7 \cdot nH_2O$ (Ln = La, Pr, Nd) samples under air flow. The number of intercalated water molecules was calculated from the weight loss from 100°C (dashed line). The first derivatives of the TGA curves are shown in the plot inset.

164.66°(NdN2). In the LnN2 series, the Ta-(O2)-Ta angle remains almost constant, independent of the H_2O/Ta ratio. For the cell parameters of the rare earth tantalates (see **Table 1**) there is no correlation between the lanthanide ionic radii (1.36, 1.31 and 1.27Å for La^{3+} , Pr^{3+} and Nd^{3+} , respectively, all them in coordination 12[32]) and the values of the a and c

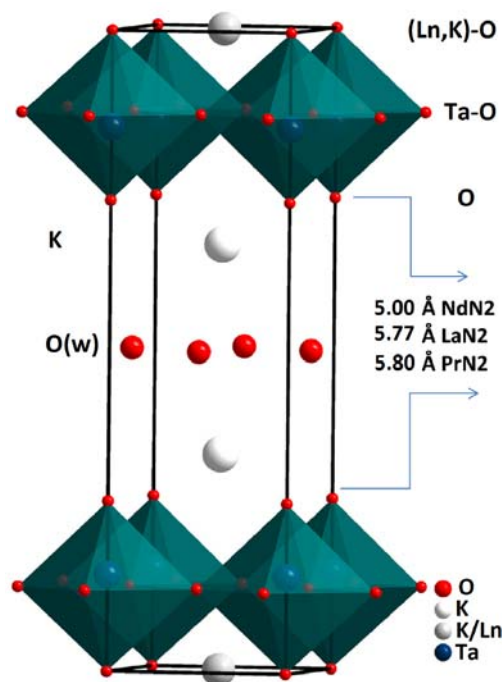


Fig. 3. Crystal unit cell of the HP of $K_2Ln_{2/3}Ta_2O_7$ (Ln=La, Pr, Nd). This figure shows the P4/mmm SG in which the water molecules (only the oxygen atom in red is shown) have been intercalated in the original I4/mmm crystal cell. The interlayer spaces of the intercalated water were evaluated from Rietveld refinements.

Table 2. Atomic and thermal parameters obtained from Rietveld refinements of the XRD data on $K_2La_{2/3}Ta_2O_7 \cdot 2.5H_2O$, $K_2Pr_{2/3}Ta_2O_7 \cdot 1.8H_2O$, and $K_2Nd_{2/3}Ta_2O_7 \cdot 0.8H_2O$ at room temperature. In these structural refinements, the SG is P4/mmm (No. 123); O(w) represent the oxygen atoms of the water molecules, and the K and Ln site occupancies were fixed to the stoichiometric values.

Compound	Atom	Site occupancy	x	y	z	100U _{iso} (Å ²)	Wyckoff Symmetry
$K_2La_{2/3}Ta_2O_7 \cdot 2.5H_2O^a$	K(2)	0.833	1/2	1/2	0.33674	0.01000	2h
	K(1)	0.333	1/2	1/2	0	0.05491	1c
	La	0.667	1/2	1/2	0	0.05491	1c
	Ta		0	0	0.15061	0.02806	2g
	O(1)		0	0	0	0.01000	1a
	O(2)		0	1/2	0.1300	0.01000	4i
	O(3)		0	0	0.28876	0.01000	2g
	O(w)		0	1/2	1/2	0.07700	2e
$K_2Pr_{2/3}Ta_2O_7 \cdot 1.8H_2O^b$	K(1)	0.333	1/2	1/2	0	0.0100	1c
	K(2)	0.833	1/2	1/2	0.32820	0.0100	2h
	Pr	0.667	1/2	1/2	0	0.0100	1c
	Ta		0	0	0.15080	0.0100	2g
	O(1)		0	0	0	0.0100	1a
	O(2)		0	1/2	0.1300	0.0100	4i
	O(3)		0	0	0.28852	0.0100	2g
	O(w)		0	1/2	1/2	0.0100	2e
$K_2Nd_{2/3}Ta_2O_7 \cdot 0.8H_2O^c$	K(1)	0.333	1/2	1/2	0	0.19222	1c
	K(2)	0.833	1/2	1/2	0.34998	0.02500	2h
	Nd	0.667	1/2	1/2	0	0.19222	1c
	Ta		0	0	0.14740	0.08297	2g
	O(1)		0	0	0	0.02500	1a
	O(2)		0	1/2	0.12569	0.02500	4i
	O(3)		0	0	0.29862	0.02500	2g
	O(w)		0	1/2	1/2	0.02500	2e

^a $a = 3.9297 \text{ \AA}$, $c = 13.6587 \text{ \AA}$, $R_{wp} = 5.77$, $\chi^2 = 2.97$.

^b $a = 3.9449 \text{ \AA}$, $c = 13.7019 \text{ \AA}$, $R_{wp} = 6.42$, $\chi^2 = 4.276$.

^c $a = 3.9864 \text{ \AA}$, $c = 12.4058 \text{ \AA}$, $R_{wp} = 3.21$, $\chi^2 = 6.757$.

parameters with the water content in the crystal structure of the HPs. Comparing the water content to LnN₂ compounds, the larger water content corresponds to the shorter distance between the slice of the TaO₆ octahedra (see **Fig. 3**). Hydrated systems that exhibit the configuration of adjacent perovskite blocks with alkaline or alkaline-earth metals in the rock salt block have been reviewed by Lehtimäki *et al*[14]. According to this study, the main factors affecting the water intercalation are: the size of cations in the rock-salt block, the oxygen content of compounds, and the valence of the transition metal in the structure.

An additional aspect of the LnN₂ crystal structure, which is defective in 1/3 of the Ln³⁺ ion per unit formula, is that we have not observed ordering of vacancies that could be shown as additional reflections in the XRD pattern. This is probably due to the particle small size of the hydrated samples and the width of reflections. For $K_2La_{2/3}Ta_2O_7$,

Crosnier-Lopez *et al*[27] observed by XRD and HRTEM, that the atomic vacancies are restricted to 9-coordinated K sites. As observed the diffraction patterns of the HP of LnN₂ (see **Fig. 1**), all of them exhibit the characteristic broad reflections associated to the presence of very small crystallites in samples. Using the Scherrer equation to evaluate the average size of the crystallite, we obtain 4 nm. By Scanning Electron Microscopy (not shown), the average size of particles is about 50 nm.

The HRTEM images of LaN₂ (**Fig. 5**) reveal the good crystallinity of the tetragonal phase, this confirms the fact that a single phase can be obtained by the synthetic route of this work. Most of the HRTEM micrographs exhibit patterns corresponding to the (110), (100), (111), (010), (011), (014) and (013) crystallographic planes, with interplanar spacings of approximately 2.82, 3.69, 2.68, 4.12, 3.67, 2.64 and 2.99Å, respectively. The incidence of these planes re-

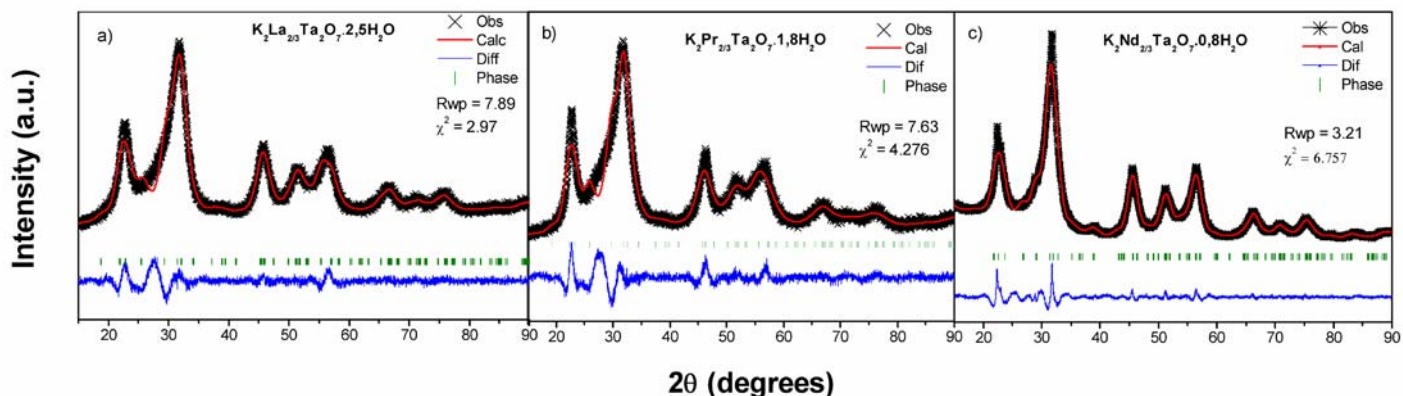


Fig. 4. Rietveld refinement plots for the HP of $K_2Ln_{2/3}Ta_2O_7$, a) Ln=La, b) Ln=Pr, and c) Ln=Nd; in these systems a P4/mmm SG was used and the intercalated water molecules between the TaO_6 octahedral slices was modeled as O(w), see **Table 1**.

veals a predominant preferential orientation[27] of crystals in the LaN2 phase. These orientations agree well with the intense reflections observed in the DRX pattern. By HRTEM, the existence of an infrequent plane was also found, the (002) plane with 6.12\AA (see **Fig. 5a** zone I, **Fig. 5e** zone I). Based on the goodness-of-fit parameters (Rp, Rwp, Rexp and χ^2) of the structural refinements and the HRTEM images, the synthesis of the HPs of $K_2Ln_{2/3}Ta_2O_7$ was confirmed.

The adsorption-desorption isotherms

To determine the specific surface area of the HP of LnN2, the BET method was used and the graphical results are presented in the **Fig. 6**. Adsorption isotherms of $K_2Ln_{2/3}Ta_2O_7$ can be associated to the type II of the IUPAC classification, which represent an unrestricted monolayer-multilayer adsorption[33]. For most of the compounds at low P/Po (~ 0.25 - 0.35) ratio, the

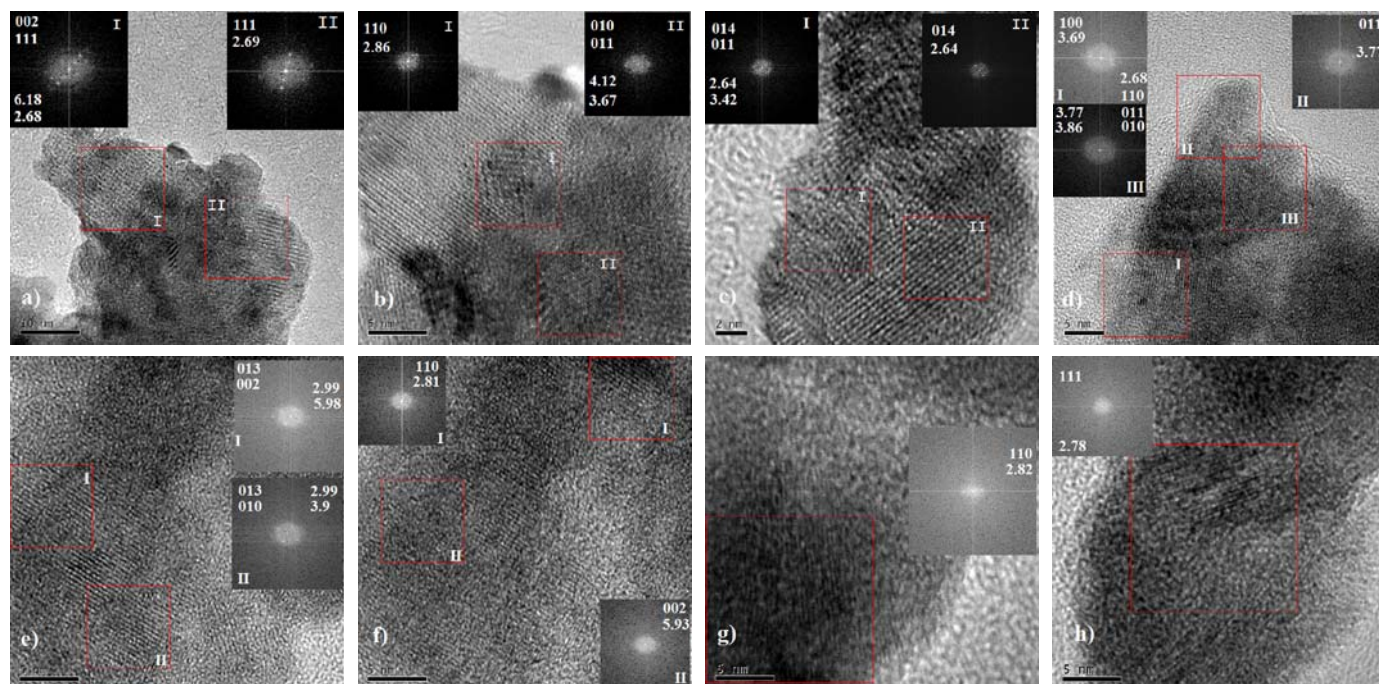


Fig. 5. HRTEM micrographs series of samples a) LaN2; b) LaN2; c) LaN2; d) PrN2; e) PrN2; f) NdN2, g) NdN2, and h) NdN2. For all the samples interplanar distances and crystallographic information have been derived after FT (Fourier Transform analysis) and displayed in the corresponding insets. Even though samples look with high levels of crystallinity, faulted structures (dislocations and stacking faults) can be observed everywhere in all the samples. These faulted structures might be related with the insertion of ions into the materials during the synthesis processes.

stage of complete monolayer coverage can be observed (see **Fig. 6**). The most relevant feature of this isotherm is that they did not exhibit any limiting adsorption at high P/P₀ ratio. This behavior can be caused by the existence of non-rigid aggregates of plate-like particles of slit-shaped pores[34]. The BET surface areas of the LnN₂ compounds of the present work are 3.0 m²/g, 3.9 m²/g, and 5.4 m²/g for the HPs of K₂Pr_{2/3}Ta₂O₇, K₂La_{2/3}Ta₂O₇, and K₂Nd_{2/3}Ta₂O₇, respectively. These values are in the order reported for K₂La_{2/3}Ta₂O₇ (3.7 m²/g), obtained by the solid state reaction method[9]. This behavior can be directly associated to the kind of cation (alkaline or alkaline-earth metals).

Absorbance spectra

To obtain the absorbance spectra of the K₂Ln_{2/3}Ta₂O₇ compounds, these were scanned in the wavelength range from 250 nm to 700 nm, using the DRS technique[35],[36]. As observed in the absorption spectra of the **Fig. 7**, for PrN₂ and NdN₂, redshifted absorption appear with maxima at 380 nm (Pr) and 585 nm (Nd). The band gaps values were calculated with the Kubelka-Munk function, and the values obtained are: 3.70 eV, 3.6 eV, and 3.5 eV for LaN₂, PrN₂, and NdN₂, respectively. These absorption signals are associated with internal transitions in the localized 4f states[37], even though they are expected to be sharp peaks. This graph (**Fig 7**), and electronic structure calculations, support[38] the incomplete localization of the Ln (Pr and Nd) 4f electrons and thus its participation in the chemical bonding via orbital hybridization in the Ln-O-Ta system, while the interlayer cations (K) have a negligible effect on the electronic structure of layered Ln-tantalates. As expected from previous considerations, in the MLnTa₂O₇ (M=Cs, Rb, Na and H; Ln=La, Pr, Nd and Sm) series, a Dion-Jacobson type system, the experimental activity in water photolysis decreases in the sequence Nd>Sm>La>Pr; the low activity in the

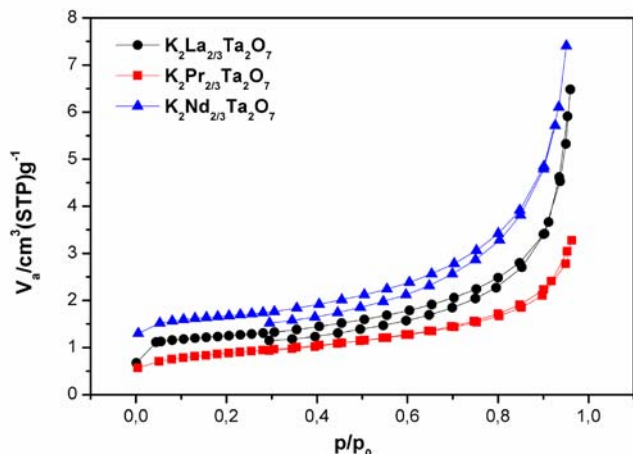


Fig. 6. Adsorption-desorption isotherms for LnN₂ (Ln = La, Pr, Nd). From this plot, the estimated values of the specific surface area are 3.9 (LaN₂), 3.0 (PrN₂) and 5.4(NdN₂) m²/g.

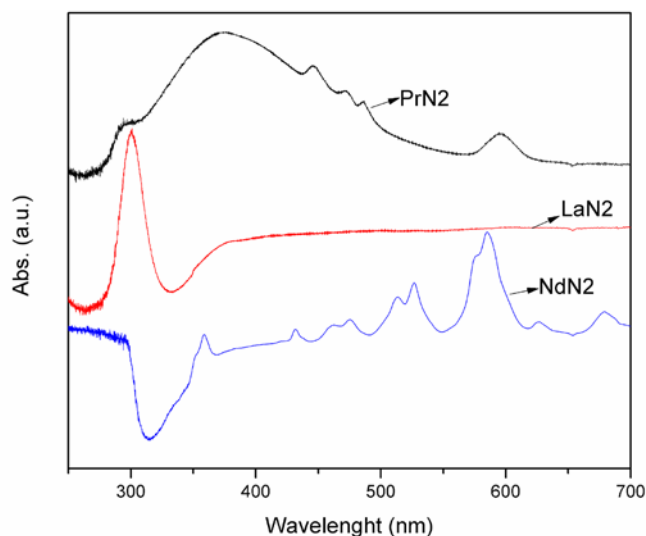


Fig. 7. UV-Vis spectra from DRS for the samples of this work, LaN₂, PrN₂ and NdN₂. As can be observed from the absorption spectra of PrN₂ and NdN₂, there is redshifted absorption whose maxima appear at 380 nm (Pr) and 585 nm (Nd).

Pr system is explained by their acting as a trapping center of electronic holes[29].

Photocatalytic activity

The photocatalytic activity of the LnN₂ compounds is presented in the graph (**Fig. 8**). The photocatalytic reaction was carried out in an inner irradiation quartz cell. The catalyst was dispersed in aqueous methanol solution (14% vol/vol), using deionized water, then it was irradiated by a high pressure Hg lamp (400W). Amounts of evolved hydrogen gas were analyzed by gas chromatography. The highest activity was achieved when the catalysts were used in aqueous methanol mixture (see **Table 3**), except to PrN₂. On the other hand, as the larger surface area corresponds to NdN₂; it is considered that the smaller particle size increases the activity for water splitting. Comparing the most active powder (NdN₂), the activity was higher by twice than that when LaN₂ and PrN₂ were used in an aqueous methanol solution (97.5 μmol H₂/g.h). When the reaction was tried in pure water (see **Table 4**), the NdN₂ compound also had higher activity than PrN₂ and LaN₂; although the NdN₂ and LaN₂ activity decreased in pure water, while that of PrN₂ remained low. Therefore, the high photocatalytic activity of the NdN₂ sample should be associated with the high specific surface area of this sample. In an analogous system, RbLnTa₂O₇ (Ln = La, Pr, Nd, Sm), Machida *et al.*[39] showed that the Nd system also exhibited the highest activity. The explanation of this activity is associated to the electronic structure change that comes out from the unfilled 4f levels of the lanthanide. The Ln-O-Ta hybridization affects the position of both; the conduction band and the valence

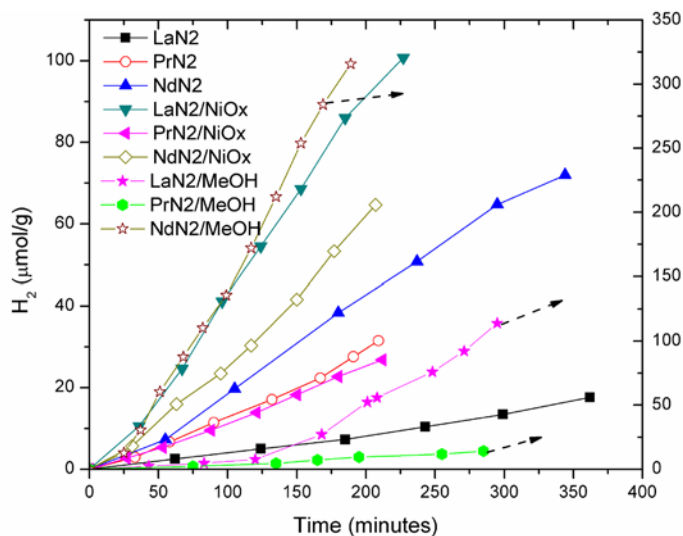


Fig. 8. Photocatalytic activity for water splitting of the LaN2, PrN2 and NdN2 compounds (deionized water, pH=7); Hydrogen evolution from 14% (vol/vol) methanol/water solution (right-side scale), and Hydrogen evolution from deionized water (left-side scale) with NiOx (0.5 wt %) as cocatalyst.

band edges, as well as their density of states (DOS)[38]. Electronic structure calculations show[37]–[39] that the unoccupied 4f (Ln = La) levels lay at the bottom of the con-

duction band, whereas the occupied 4f levels become lowered as the number of 4f electrons increases. Finally, these levels overlap with O-2p band for Ln = Nd and Sm[37]. In this way, the presence of empty Ln-4f bands is a possible reason for the low level of the conduction band edge. This empty 4f bands are not necessarily manifested as a drop in the band gap values, but these states can act as ‘stepping stones’ for the electrons to jump to the conduction band[38]. Previous results on the photocatalytic activity of the layered tantalates $RbLnTa_2O_7$ (Ln = La, Pr, Nd, and Sm) [24],[39], with different cation arrangement between two contiguous perovskite slabs, account for the H_2 evolution over the catalysts; 6, 4.2, and 47 for La, Pr, and Nd, respectively (all in units of $mmol \cdot h^{-1}$ for 1 g of catalyst). As a matter of comparison, when the NiOx loading was performed, the photocatalytic activity was notably improved, as reported by Shimizu et al. [9]. When NiOx was loaded onto the $H_2La_{2/3}Ta_2O_7$ and $K_2La_{2/3}Ta_2O_7$ surfaces, the hydrogen evolution increased by about ten times in the first compound (from 146 to 940 $mmol \cdot h^{-1}$). In the present work, the hydrogen evolution on the NiOx-LaN2 sample increased from 2.9 to 26.6 $\mu mol \cdot h^{-1}$, and it was the highest increment observed in the photocatalytic activity.

In order to explore the NiOx-cocatalyst effect on the H_2 production of the LnN2 samples, NiOx-loaded LnN2 compounds were performed. The H_2 evolution rates of the LaN2 and NdN2 samples were significantly increased by the addi-

Table 3. Photocatalytic activity obtained in a 14 % methanol/water solution.

$K_2La_{2/3}Ta_2O_7$ in 14% methanol/water solution		$K_2Pr_{2/3}Ta_2O_7$ in 14% methanol/water solution		$K_2Nd_{2/3}Ta_2O_7$ in 14% methanol/water solution	
Time (min)	H_2 ($\mu mol/g$)	Time (min)	H_2 ($\mu mol/g$)	Time (min)	H_2 ($\mu mol/g$)
0	0	0	0	0	0
43	2.38	75	2.14	25	12.7
83	4.59	135	4.44	37	30.59
120	7.53	165	7.16	51	60.35
168	27.19	195	9.41	68	87.67
201	52.34	255	11.75	82	110.21
208	55.80	285	14.09	99	135.61
248	75.91			117	172.07
271	92.17			135	212.13
295	113.91			153	253.88
				169	284.07
				189	315.78

Table 4. Photocatalytic activity obtained in water deionized.

$K_2La_{2/3}Ta_2O_7$ in water		$K_2Pr_{2/3}Ta_2O_7$ in water		$K_2Nd_{2/3}Ta_2O_7$ in water	
Time (min)	H_2 ($\mu mol/g$)	Time (min)	H_2 ($\mu mol/g$)	Time (min)	H_2 ($\mu mol/g$)
0	0	0	0	0	0
62	2.54	33	2.90	55	7.27
124	5.00	58	6.64	105	19.73
185	7.29	90	11.45	180	38.32
243	10.37	132	17.07	237	50.77
299	13.41	167	22.34	295	64.77
362	17.61	191	27.57	344	71.97
		209	31.53		

tion of NiOx (0.5 wt %) as cocatalyst (**Fig. 8, Table 5**). In contrast to this behavior, the NiOx loading of the PrN2 sample resulted in a small decrease of the activity. However, the increase of NiOx-LaN2 activity was higher than the other compounds (from 2.92 $\mu\text{mol H}_2/\text{g.h}$ to 26.63 $\mu\text{mol H}_2/\text{g.h}$). The higher activity of the NiOx-loaded compounds is due to the type of heterojunction formed at the semiconductor interface[40]. When NiOx and LnN2 are brought into contact, their Fermi levels align, due to the charge transfer phenomenon. Therefore, under illumination, the LnN2 compounds produce electron diffusion across the depletion region to the NiOx for H_2 evolution. When the NiOx cocatalyst is pre-treated under H_2 reduction conditions, and then a subsequent O_2 oxidation, a NiO/Ni double layer structure is produced, and the electron transference to the photocatalyst active sites is facilitated.

Conclusions

By the polymeric complex method, we successfully synthesized isostructural layered perovskite tantalates which correspond to the hydrated phases of $\text{K}_2\text{Ln}_{2/3}\text{TaO}_7$ (Ln=La, Pr, Nd). These compounds are 1/3 Ln-deficient Ruddlesden-Popper systems of layered tantalates. Rietveld structural refinements and HRTEM images confirm the synthesis of Ln-deficient double-perovskite tantalates. The $\text{K}_2\text{Ln}_{3/2}\text{Ta}_2\text{O}_7$ (Ln = La, Pr, Nd) systems have a large ability to intercalate water molecules. This has been experimentally proved to be important in water splitting. According to the absorption-desorption isotherms, the higher surface area was obtained in the NdN2 compound. The DRS plot shows maxima absorption at 380 nm (Pr) and 585 nm (Nd), and this seems to depend on the nature of the lanthanide (La, Pr, Nd) in the crystal structure. The higher photocatalytic activity was observed in the NdN2 compound and it increased when NiOx cocatalyst was loaded on the surface of powders. Finally, the H_2 evolution was higher when the reaction was carried out in an aqueous methanol mixture, due to the sacrificial reagent effect (except to PrN2). Layered lanthanide tantalates, particularly the Nd layered tantalate, are suitable compounds to reach high photocatalytic activity in water splitting. Through the experiments of this work, the role played by the Ln-deficien-

cies in the crystal structure is not clear and further experiments are needed in this direction.

Experimental

Preparation of samples

Samples with the general formula $\text{K}_2\text{Ln}_{2/3}\text{Ta}_2\text{O}_7$, with Ln = La, Pr, and Nd, were prepared by the Pechini method[41]–[43] in which nitrates of the respective lanthanides ($\text{La}(\text{NO}_3)_3 \cdot 6\text{H}_2\text{O}$, $\text{Nd}(\text{NO}_3)_3 \cdot 6\text{H}_2\text{O}$ and $\text{Pr}(\text{NO}_3)_3 \cdot 6\text{H}_2\text{O}$ (all of them Aldrich, 99.9%); tantalum chloride (TaCl_5 , Aldrich, 99.99%); and potassium carbonate (K_2CO_3 , Aldrich, 99.995%) were dissolved in methanol in the cationic proportion 2:2/3:2. An excess, 100 % of K_2CO_3 , was added to compensate for the volatility of the oxide form at high temperature. Then, the temperature was increased to 80°C and ethylene glycol was added to facilitate the solubility of salts. The solution was fully translucent and free of precipitates and suspended particles. At this step and with vigorous stirring, citric acid was added to enhance the solubility and form a condensation polymer until the solution became a viscous brown gel. These gels were slowly heated in a high-alumina crucible to 450°C for two hours, then black, highly porous, solids were formed. These solids were then finely ground for a subsequent calcination at 850°C for 48 hours. Subsequently, the compounds were suspended in water with stirring for approximately 30 minutes to dissolve the potassium excess and obtain the hydrated phases. The resulting HPs of the lanthanide tantalates were $\text{K}_2\text{La}_{2/3}\text{Ta}_2\text{O}_7$ (LaN2) (white powders); $\text{K}_2\text{Nd}_{2/3}\text{Ta}_2\text{O}_7$ (NdN2) (pale-purple powders) and $\text{K}_2\text{Pr}_{2/3}\text{Ta}_2\text{O}_7$ (PrN2) (pale-yellow powders). As previously reported by Crosnier-Lopez[27] for $\text{K}_2\text{La}_{2/3}\text{Ta}_2\text{O}_7$, the Ln-tantalates undergo rapid hydration when the samples are stored under room temperature conditions. Therefore, the crystal structure, X-ray diffraction (XRD), High Resolution Transmission Electron Microscopy (HRTEM)), specific surface area, thermal analysis, and photocatalytic activity characterization of the samples of this work, correspond to the hydrated form of the lanthanide tantalates, $\text{K}_2\text{Ln}_{2/3}\text{Ta}_2\text{O}_7$ (LnN2) (Ln = La, Pr, Nd). NiOx-Loaded catalysts were prepared by impregnation of

Table 5. Photocatalytic activity of the compounds loaded with NiOx over water deionized.

$\text{K}_2\text{La}_{2/3}\text{Ta}_2\text{O}_7/\text{NiOx}$ in water		$\text{K}_2\text{Pr}_{2/3}\text{Ta}_2\text{O}_7/\text{NiOx}$ in water		$\text{K}_2\text{Nd}_{2/3}\text{Ta}_2\text{O}_7/\text{NiOx}$ in water	
Time (minutes)	H_2 ($\mu\text{mol/g}$)	Time (minutes)	H_2 ($\mu\text{mol/g}$)	Time (minutes)	H_2 ($\mu\text{mol/g}$)
0	0	0	0	0	0
36	10.54	27	2.73	31	5.70
67	24.63	53	5.34	63	15.95
96	41.13	88	9.54	95	23.46
124	54.49	121	13.88	117	30.32
153	68.58	150	18.25	150	41.55
185	85.97	180	22.71	177	53.32
227	100.76	212	26.84	207	64.67

the samples (2g) with an aqueous solution of $Ni(NO_3)_2 \cdot 6H_2O$ (Aldrich, 99.99%). After stirring for 30 minutes, the water was evaporated in an oven. The powders were dried at 80°C for 4 h and then calcined at 350°C for 1 h, and then at 450°C for 2 h in air. Subsequently, the catalysts were reduced in a H_2 atmosphere at 500 °C for 2 h, and oxidized in O_2 atmosphere at 200°C for 1 h to produce NiO/Ni clusters (NiOx).

Characterization

XRD patterns of powders were gathered using a Siemens D-5000 diffractometer in a Bragg-Brentano geometry configuration ($CuK_{\alpha 1}$ radiation, $\lambda = 1.5406 \text{ \AA}$), in air at room temperature (RT), with the operating conditions of 35kV and 35 mA. For the three hydrated compounds, the scanning angular range was $6^\circ \leq 2\theta \leq 90^\circ$ with a step scan of $0.02^\circ/10$ seconds. Rietveld analyses were performed using the General Structure Analysis System[44] (GSAS Package) code with the graphical user interface EXPGUI[45]. After full hydration of the samples by continuous washing with deionized water, thermogravimetric analyses (TGA) were performed using a TGA Q50 (TA Instruments) with a heating rate of $10^\circ C/min$ in airflow, from RT to $1000^\circ C$.

HRTEM analyses of hydrated samples were performed using a JEOL 2010-TEM/STEM microscope operated at 200 kV. The samples were softly ground to obtain fine powders and then dispersed in deionized water using an ultrasonic bath. A drop of this suspension was placed on a carbon-coated copper grid. Crystallographic information for the compounds was derived from the HRTEM micrographs and studied and analyzed using the commercial Digital Micrograph computing programme[46]. The electronic spectra (diffuse reflectance) were measured on a Cary 5E UV-Vis-NIR spectrophotometer in the 250-700 nm range. To determine the surface area, N_2 adsorption-desorption isotherms were obtained using a Bel Japan Minisorp-II instrument. All the samples were previously degassed at $200^\circ C$ under vacuum conditions for 4 hours. The photocatalytic activity was measured by hydrogen evolution with an inner irradiation cell made of quartz. The catalyst (1 g) was dispersed in aqueous methanol solution (14%) and deionized water by magnetic stirring and was irradiated by a high pressure Hg lamp (400W). Amounts of evolved gases were analyzed by gas chromatography (Varian Aerograph 1400, Ar carrier, stainless steel column 40/60 mesh) through a gas sampler (3 cm^3) which was directly connected to the reaction system to avoid any contamination from air.

Acknowledgements

The authors thank M in C. Cecilia Salcedo-Luna (USAI-FQU-NAM) for her help in the XRD experiments. This work was partially supported by the PAPIIT projects IN- 118710 and IN-214313. HV-S gratefully acknowledges the financial support from DGAPA (UNAM).

References

- Ruddlesden, S. N.; Popper, P. *Acta Crystallogr.* **1957**, *10*, 538-539.
- Ollivier, P. J.; Mallouk, T. E. *Chem. Mater.* **1998**, *10*, 2585-2587.
- Schaak, R. E.; Mallouk, T. E. *Chem. Mater.* **2002**, *14*, 1455-1471.
- Toda, K.; Watanabe, J.; Sato, M. *Mater. Res. Bull.* **1996**, *31*, 1427-1435.
- Toda, K.; Teranishi, T.; Ye, Z. G.; Sato, M.; Hinatsu, Y. *Mater. Res. Bull.* **1999**, *34*, 971-982.
- Schaak, R. E.; Mallouk, T. E. *Chem. Mater.* **2000**, *12*, 3427-3434.
- Shimizu, K.; Itoh, S.; Hatamachi, T.; Kitayama, Y.; Kodama, T. *J. Mater. Chem.* **2006**, *16*, 773.
- Tahara, S.; Ichikawa, T.; Kajiwaru, G.; Sugahara, Y. *Chem. Mater.* **2007**, *19*, 2352-2358.
- Shimizu, K. I.; Itoh, S.; Hatamachi, T.; Kodama, T.; Sato, M.; Toda, K. *Chem. Mater.* **2005**, *17*, 5161-5166.
- Mitsuyama, T.; Tsutsumi, A.; Sato, S.; Ikeue, K.; Machida, M. *J. Solid State Chem.* **2008**, *181*, 1419-1424.
- Ida, S.; Okamoto, Y.; Hagiwara, H.; Ishihara, T. *Catalysts* **2013**, *3*, 1-10.
- Schottenfeld, J. A.; Kobayashi, Y.; Wang, J.; Macdonald, D. D.; Mallouk, T. E. *Chem. Mater.* **2008**, *20*, 213-219.
- Josepha, E. A.; Wiley, J. B. Topochemical Manipulation of Layered Perovskites, University of New Orleans Theses and Dissertations. **2011**, Vol. PhD.
- Lehtimäki, M.; Yamauchi, H.; Karppinen, M. *J. Solid State Chem.* **2013**, *204*, 95-101.
- Gopalakrishnan, J.; Bhat, V. *Inorg. Chem.* **1987**, *26*, 4299-4301.
- Shimizu, K.; Tsuji, Y.; Kawakami, M.; Toda, K.; Kodama, T.; Sato, M.; Kitayama, Y. *Chem. Lett.* **2002**, No. 11, 1158-1159.
- Shimizu, K.; Tsuji, Y.; Hatamachi, T.; Toda, K.; Kodama, T.; Sato, M.; Kitayama, Y. *Phys. Chem. Chem. Phys.* **2004**, *6*, 1064.
- Kudo, A.; Miseki, Y. *Chem. Soc. Rev.* **2009**, *38*, 253-278.
- Kudo, A.; Kato, H. *Chem. Phys. Lett.* **2000**, *331*, 373-377.
- Kudo, A. *Pure Appl. Chem.* **2007**, *79*, 1917-1927.
- Kudo, A.; Kato, H.; Tsuji, I. *Chem. Lett.* **2004**, *33*, 1534-1539.
- Kato, H.; Kudo, A. *Catal. Letters.* **1999**, *58*, 153-155.
- Kato, H.; Asakura, K.; Kudo, A. *J. Am. Chem. Soc.* **2003**, *125*, 3082-3089.
- Machida, M.; Yabunaka, J.; Kijima, T. *Chem. Mater.* **2000**, *12*, 812-817.
- Kudo, A.; Okutomi, H.; Kato, H. *Chem. Lett.* **2000**, 1212-1213.
- Le Berre, F.; Crosnier-Lopez, M. P.; Fourquet, J. L. *Mater. Res. Bull.* **2006**, *41*, 825-833.
- Crosnier-Lopez, M. P.; Le Berre, F.; Fourquet, J. L. *Z. Anorg. Allg. Chem.* **2002**, *628*, 2049-2056.
- Le Berre, F.; Crosnier-Lopez, M. P.; Laligant, Y.; Fourquet, J. L. *J. Mater. Chem.* **2002**, *12*, 258-263.
- Machida, M.; Miyazaki, K.; Matsushima, S.; Arai, M. *J. Mater. Chem.* **2003**, *13*, 1433.
- Crosnier-Lopez, M. P.; Le Berre, F.; Fourquet, J. L. *J. Mater. Chem.* **2001**, *11*, 1146-1151.
- Richard, M.; Brohan, L.; Tournoux, M. *J. Solid State Chem.* **1994**, *112*, 345-354.
- Shannon, R. D. *Acta Crystallogr. Sect. A.* **1976**, *32*, 751-767.
- Sing, K. S. W. Reporting physisorption data for gas/solid systems with special reference to the determination of surface area and porosity (Recommendations 1984). *Pure and Applied Chemistry*, **1985**, *57*, 603-619.

34. Thommes, M. *Chemie-Ingenieur-Technik*. **2010**, 82, 1059-1073.
35. Li, D.; Zheng, J.; Li, Z.; Fan, X.; Liu, L.; Zou, Z. *Int. J. Photoenergy*. **2007**, 2007, 1-7.
36. Luan, J.; Cai, H.; Zheng, S.; Hao, X.; Luan, G.; Wu, X.; Zou, Z. *Mater. Chem. Phys.* **2007**, 104, 119-124.
37. Machida, M.; Yabunaka, J.; Kijima, T.; Matsushima, S.; Arai, M. *Int. J. Inorg. Mater.* **2001**, 3, 545-550.
38. Ramirez-De-Arellano, J. M.; Ruiz-Chavarría, S.; Valencia-Sánchez, H.; Tavizon, G.; De La Mora, P. *Comput. Mater. Sci.* **2014**, 93, 160-163.
39. Machida, M.; Yabunaka, J.; Kijima, T. *Chem. Commun.* **1999**, 1939-1940.
40. Hu, C. C.; Teng, H. *J. Catal.* **2010**, 272, 1-8.
41. Yoshino, M.; Kakihana, M.; Cho, W.; Kato, H.; Kudo, A. *Chem. Mater.* **2002**, 14, 3369-3376.
42. Takahashi, H.; Kakihana, M.; Yamashita, Y.; Yoshida, K.; Ikeda, S.; Hara, M.; Domen, K. *J. Alloys Compd.* **1999**, 285, 77-81.
43. Ikeda, S.; Hara, M.; Kondo, J. N.; Domen, K.; Takahashi, H.; Okubo, T.; Kakihana, M. *Chem. Mater.* **1998**, 10, 72-77.
44. Larson Von Dreele, R.B, a C. General Structure Analysis System (GSAS), 1994, Los Alamos National Laboratory.
45. Toby, B. H. *J. Appl. Crystallogr.* **2001**, 34, 210-213.
46. Team, G. S. DigitalMicrograph 3.7.0 for GMS 1.2, **1999**.